Comparison of three coarsening methods of gridded digital elevation models by ParFlow.CLM in a typical karstic basin of Central China

Zitong Jia[1], Chen Yang[2], and Wei Liu[3]

[1]China University of Geosciences, Wuhan
[2]Princeton University
[3]China University of Geosciences (Wuhan)

December 7, 2022

Abstract

Extraction of critical hydrologic features from high-resolution topographic data is challenging using existing grid coarsening approaches, such as surface flow path, river network, and slope, which limits the application of hydrological models. In this research, the influence of various grid coarsening techniques on the prediction outcomes was measured by a numerical experiment based on the integrated hydrological model ParFlow-Common Land Model (ParFlow.CLM). Three grid coarsening methods (Nearest Neighbor Coarsening, Majority Coarsening, Hydrography-Driven Coarsening) were applied to simulate evapotranspiration(E), soil temperature(ST), streamflow, soil moisture(SM) and latent(LE) heat fluxes in central China's Sixi Valley, a classic example of a karstic basin. As a result, the three grid coarsening methods perform uniform in simulating latent heat fluxes and soil temperature. However, their ability to predict soil moisture surface flow and evapotranspiration are more diverging. The hydrography-driven coarsening extracts significantly more accurate valleys, rivers network, and slopes closer to the actual terrain than existing coarsening strategies. Slopes derived from hydrography-driven coarsening methods can be used to predict more accurately the top soil moisture, evapotranspiration, and streamflow dynamics processes. This study stresses that a hydrography-driven coarsening strategy is advocated for all those cases in which topographic slope extracted using a coarse-grid digital elevation model is an important influence on the ParFlow.CLM simulation of essential hydrographic features.

Hosted file

`essoar.10512947.1.docx` available at https://authorea.com/users/564241/articles/611177-comparison-of-three-coarsening-methods-of-gridded-digital-elevation-models-by-parflow-clm-in-a-typical-karstic-basin-of-central-china

1

Comparison of three coarsening methods of gridded digital elevation models by ParFlow.CLM in a typical karstic basin of Central China

Zitong Jia[1], Chen Yang[2], Wei Liu[1, *]

1. Institute of Geological Survey, China University of Geosciences, Wuhan 430074, China

2. Department of Civil and Environmental Engineering, Princeton University, Princeton, NJ 08544, USA

*Corresponding author, e-mail: wliu@cug.edu.cn

Abstract: Extraction of critical hydrologic features from high-resolution topographic data is challenging using existing grid coarsening approaches, such as surface flow path, river network, and slope, which limits the application of hydrological models. In this research, the influence of various grid coarsening techniques on the prediction outcomes was measured by a numerical experiment based on the integrated hydrological model ParFlow-Common Land Model (ParFlow.CLM). Three grid coarsening methods (Nearest Neighbor Coarsening, Majority Coarsening, Hydrography-Driven Coarsening) were applied to simulate evapotranspiration(E), soil temperature(ST), streamflow, soil moisture(SM) and latent(LE) heat fluxes in central China's Sixi Valley, a classic example of a karstic basin. As a result, the three grid coarsening methods perform uniform in simulating latent heat fluxes and soil temperature. However, their ability to predict soil moisture surface flow and evapotranspiration are more diverging. The hydrography-driven coarsening extracts significantly more accurate valleys, rivers network, and slopes closer to the actual terrain than existing coarsening strategies. Slopes derived from hydrography-driven coarsening methods can be used to predict more accurately the top soil moisture, evapotranspiration, and streamflow dynamics processes. This study stresses that a hydrography-driven coarsening strategy is advocated for all those cases in which topographic slope extracted using a coarse-grid digital elevation model is an important influence on the ParFlow.CLM simulation of essential hydrographic features.

Keywords: ParFlow.CLM; Grid coarsening methods inter-comparison; karst; the significance test of EEMD

1 Introduction

Gridded digital elevation models(DEM) are used to characterize terrain and extract hydrologic properties. Physically based hydrological model simulations usually require a topographic computational grid input to ensure that drainage networks are connected in the model simulation to obtain slope values (Condon & Maxwell, 2019). The most commonly used hydrological terrain attributes are specific catchment area, surface flow path, river flow network, and slope (Gallant & Hutchinson, 2011). In predicting depict surface water flow dispersion, extracting watershed hydrologic features, and offering precise topographic descriptions of hillslopes, a wide variety of algorithms have been utilized to handle dem data in grid-based digital elevation models (Barnes et al.,2014; Orlandini

and Moretti, 2009a, 2009b; Kenny et al., 2008). Chosen the suitable coarsening grid method is essential for large-scale and long-term hydrologic simulations due to their high computing demands.

The level of coarsening of the grid and the resolution size significantly impact the timing and accuracy of model runs. Hydrologic parameters, including slope, stream velocity, and drainage patterns are all susceptible to change when the spatial resolution of a DEM is reduced (Tang, 2000). Runoff, infiltration, evapotranspiration, and surface-subsurface exchange fluxes must be accurately simulated, however, this cannot be done without a sufficiently fine mesh grid due to the uncertainty in the coarsened grid's description of the hydrological features. (Vazquez et al., 2002; von Gunten et al., 2014). Using a well-thought-out grid coarsening strategy can improve the accuracy of model simulations. In hydrological model simulations, the nearest neighbor sampling technique frequently reses digital elevation models and the majority resampling method is rarely applied (De Bartolo et al., 2016). In contrast, when data from a high-resolution grid are coarsened to a standard rectangular grid, the nearest neighbor resampling coarsening method may produce half-image position shifts, and some hydrological line features on the original map will be transformed into erratic block features, additionally, the hydrologic features shown in the high-resolution digital elevation model are not accurately captured. (Hester & Doyle, 2008a, 2008b; Orlandini & Moretti, 2009a, 2009b; Moretti & Orlandini, 2018).

To create a drainage-limited TIN while still preserving the primary terrain characteristics, Zhou and Chen (2011) presented a compound approach based on the combination of point addition and feature point methods to extract critical points of the terrain surface from the DEM. When coarsening a high-resolution digital elevation model, the Compound Method (CM) is less accurate than Nearest Neighbor (NN) Coarsening for grid cell sizes less than 100, and the accuracy of CM coarsening is essentially equivalent to NN coarsening for grid cell sizes more than 100. (Orlandini & Moretti, 2018). Among the existing studies, Orlandini and Moretti (2018) proposed a novel approach to coarsening based on hydrography. To get channel networks out of a gridded DEM, the studied coarsening procedure comprises depression filling, slope direction, and channel initiation (Orlandini et al., 2012). This study improves on the hydrography-driven coarsening method by using the priority flood depression filling algorithm (Lindsay, 2016) and using the D4 algorithm to connect drainage networks (Orlandini et al., 2003) replace the D8-LTD slope direction algorithm (Condon & Maxwell, 2019). The DEM is converted to slopes required by the hydrologic model, and the slopes are processed to improve hydrologic modeling performance by a combination of these two algorithms. The coarsening of a gridded digital elevation model in a karst trough is performed using the enhanced hydrography-driven coarsening approach.

Specific hydrogeological condition of karst controls the complex water cycle there. Although it is generally acknowledged that subsurface flow dominates runoff in karst areas, the specific subsurface runoff paths, flow residence times,

and groundwater flow sources remain unknown (Kirchner, 2006). It is crucial to correctly identify topographic features, river networks, and other hydrological elements from the grid digital elevation model to quantify and comprehend the links between karst terrain and the hydrological cycle processes. (McGuire & McDonnell, 2010).

The connection between slope and river channel network depends on the soil characteristics, surface vegetation type, and bedrock topography of the study area (Jencso et al., 2009; McGuire & McDonnell, 2010). Climate parameters (rainfall, air temperature, atmospheric pressure) determine the distribution of surface water, whereas infiltration conditions at the surface and the amount of precipitation determine the distribution of groundwater. A crucial aspect of any hydrological modeling of a basin is accounting for how surface water and groundwater interact. Hydrological simulation tools must consider this interaction to provide reliable simulations (Kollet & Maxwell, 2006). Therefore, this study uses a parallel, three-dimensional, integrated hydrologic model called ParFlow to simulate both surface and subsurface flow (saturated and unsaturated zone) simultaneously in 3D. (Ashby & Falgout, 1996; Maxwell 2013; Kollet & Maxwell, 2006; Jones & Woodward 2001; Maxwell & Miller, 2005; Maxwell et al., 2014). On the other hand, other hydrological models usually adopt surface routing schemes for separate channels (pre-defined stream reaches) that are not considered to the impact of subsurface flow and the grid resolution (O'Neill et al., 2020; Soltani et al., 2022). ParFlow couples the common land model (CLM) into the model (Dai et al., 2003), streams form naturally as surface water is routed by topography, extending the model to consider the energy balance between land surface soils and the atmosphere and the quantitative relationship between shallow soil moisture and surface heat fluxes and temperature (Hein et al, 2019).

In this present study, three different grid coarsening methods were adopted to convert high-resolution topographic data to coarse grid digital elevation models in a typical sub-basin of a karst trough area, and numerical simulations were conducted using the integrated hydrological model ParFlow.CLM. The study has the following objectives: (1) convert high-resolution topographic data to coarse grid digital elevation models by using Hydrography-Driven Coarsening(HD), Majority Coarsening(MJ) and Nearest Neighbor Coarsening(NN) and evaluate the reality of the obtained digital elevation models and the extracted drainage networks from HD, MJ, NN coarsening methods. (2) quantify and evaluate the effect of using different coarsening methods simulated evapotranspiration(ET), soil temperature(ST), streamflow, soil moisture(SM) and latent (LE) heat fluxes in ParFlow.CLM. (3) assessing the performance of three coarsening methods applied in ParFlow.CLM on the simulated water balance of karst systems by the EEMD significance tests and six performance metrics.

2 Site description

The Sixi Valley is upstream of the Maoping River, the first tributary of the Yangtze River in the Three Gorges Reservoir, 9km Southwest of the Three

Gorges Dam, in Zigui, Yichang, Central China. Its catchment area is 48.12km², drainage density 0.65 km/km², and the average slope ratio is 0.09. The study area combines karst depressions and karst troughs and is characterized by steep terrain of middle-low mountains and deep ravines. Carbonate rocks are widely distributed in the Sixi Valley, accounting for about 70% of the study area. The surface of the geological hillside are composed of shallow soils with an average depth of 0.3m (Figure 1).
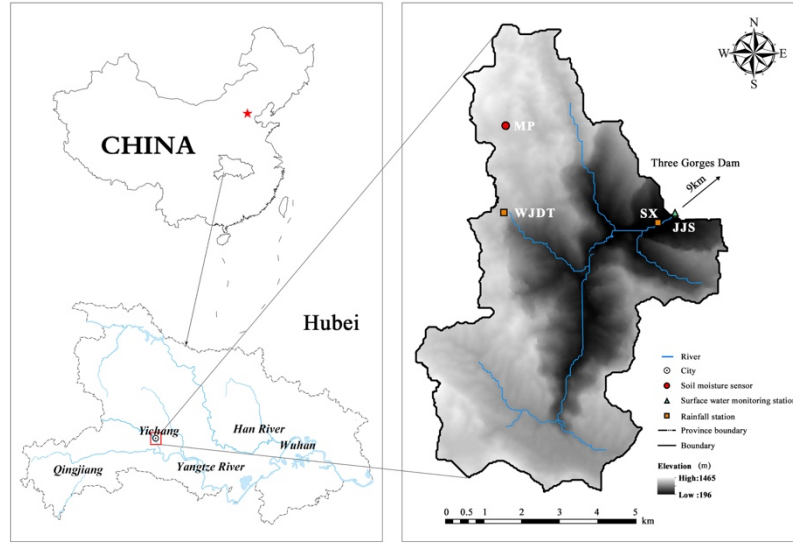

Figure 1. the modeling area in this study

3 Method

3.1 Nearest Neighbor Coarsening

The nearest neighbor coarsening (NN) is a resampling technique for raster data which the elevation of each cell center on the output raster is calculated by using the elevation of the nearest cell center on the input raster (Moretti & Orlandini 2018). When multiple cell centers in the input raster are found to be equidistant from the output raster cell centers, the average elevation on equally distant input cells is assigned to the output cell centers. NN does not change the values of the input cells.

3.2 Majority Method Coarsening

The majority(MJ) coarsening method is suitable for discrete data which has a smoother appearance than the nearest neighbor coarsening method. With MJ, the common values in grids are used to calculate the elevation of each cell center in an output raster. The majority(MJ) resampling method calculates the elevation by finding the corresponding 4 x 4 cell value in the input raster closest to the center of the cell value and assigning the output cell value using

4

the majority of the 4 x 4 neighboring points.

3.3 Hydrography-Driven Coarsening

The hydrology-driven(HD) coarsening method is proposed by Moretti and Orlandini (2018) to transfer the basic hydrographic features of river networks and valleys observed in high-resolution topographic (DEM) data directly to a coarse-grid digital elevation model. This method preserves the structure of the drainage network and reduces the impact of depression filling. The first step is processing the high-resolution digital elevation data by removing pits and filling depressions using the priority-flood depression-filling algorithm (Zhou et al., 2016; Barnes et al., 2014).

The priority flooding algorithm is a computationally efficient method of ensuring the minimum elevation adjustment required for surface drainage by filling pits sequentially from the outer edge inwards. The priority queue is sorted by lower elevation cells with higher priority, the lowest elevation cell in the queue is always the first cell to be processed for depression filling.

The D8-LTD slope direction algorithm proposed by Orlandini et al. (2003) used in the original method is replaced by the D4 connected stream network method to calculate slope direction, i.e., the grid cell with the lowest elevation is selected from the priority queue and the elevation of its unprocessed D4 neighboring cells is adjusted to ensure that they can flow to the selected grid cell(the basin has multiple outlet units, a flow channel is constructed using the R results in the basin has only one outlet unit). The purpose of using this method is to be consistent with the ParFlow hydrological model application (Condon & Maxwell, 2019).

In the second step, a hydrography-driven coarse-resolution digital elevation model is generated by using the high-resolution digital elevation model and the hydrological features observed in the associated grid network. The elevation of the center of each output grid cell is set equal to the elevation of the nearest point along the highest order flow path observed in the output cell. This value (Z_{HD}) is equal to between the minimum elevation (Z_{min}) and maximum elevation (Z_{max}) of the high-resolution grid cell located within the coarse grid cell.

3.4 Hydrological model: Parflow.CLM

ParFlow represents variably saturated three-dimensional subsurface flow by solving the Richards (1931) equation (equation 1) and combines it with surface flow by solving the two-dimensional kinematic wave equation and free-surface boundary conditions to enable the simulation of hillslope runoff and channel routing in a truly integrated way (Kollet & Maxwell, 2006; Condon & Maxwell, 2015; Yang et al., 2020). ParFlow uses the van Genuchten relationships for soil moisture and relative permeability (equations 2 and 3), and these relationships replace the Clapp and Hornberger relationships used by CLM (Clapp & Hornberger 1978).

The two models communicate over the 10 soil layers in CLM 3.0 (Dai et al., 2003) with the uppermost cell layer in ParFlow corresponding to the first soil layer below the ground surface in CLM. ParFlow calculated hydraulic pressure solution (equation 1) over the entire domain, soil saturation is calculated from the hydraulic pressure solution with the water content at the upper 10 layers passed back to CLM, where soil surface temperatures (Ts), soil and canopy evapotranspiration, plant transpiration, heat fluxes and energy balances are calculated (Maxwell et al., 2015; Condon & Maxwell, 2014a, 2014b; Yang et al., 2020; Maxwell & Miller, 2005). ParFlow.CLM is an open source, integrated surface and subsurface model (https://github.com/parflow/parflow) designed to run on massively parallel processor computer systems.

(1)

where $h(p)$ is the water saturation for hydraulic pressure p, is the water density, is the porosity of the medium, $k(x)$ is the absolute permeability of the medium, is the viscosity, $kr(p)$ is the relative permeability, q represents source terms, and z is the elevation. The saturation-pressure and relative permeability-saturation functions are represented by the van Genuchten (1980) relationships

(2)

(3)

where and n are soil parameters, S_{sat} is the saturated water content, and S_{res} is the residual saturation.

3.5 Modeling Domain

High-resolution (1 m or less) topographic data were coarsened to the coarse-resolution grid digital elevation model (100m) by three coarsening methods, and the resolution of 100m accurately captures the hydrological and geological features of the study area, while meeting computational constrains in detailed, large-scale, and long-term hydrologic simulations. The model is divided into a rectangular grid of 88×123 in the horizontal direction (nx=88, ny=123). Since the study area is a karst trough valley area with thin soil formation on both slopes and the bottom depression contains sedimentary soil with increased soil layer thickness, With the terrain following grid (Maxwell, 2013), which divides the subsurface into 6 layers in the vertical direction. The thickness of each layer is 0.2, 0.3, 0.5, 0.5, 2.5 and 105 m. The vertical resolution of the model domain was set to 1 m. The study simulated two hydrological years (2018, 2021) using hourly simulation time steps.

3.6 Model Input Data sources

The hydrometeorological data are largely unavailable for the study area, the meteorological forcing data of the long-wave radiation (DLWR; W/m^2), precipitation (APCP; mm/s), air temperature (Temp; K), specific humidity (SPFH; kg/kg), atmospheric pressure (Press; pa), East-West wind speed (UGRD; m/s), and South-to-North wind speed (VGRD; m/s), Visible

or short-wave radiation (DSWR; W/m^2) are from the ERA-5 reanalysis dataset(https://cds.climate.copernicus.eu/). ERA5 is the fifth generation ECMWF reanalysis for the global climate and weather with a spatial resolution of 0.25°×0.25 ° (atmospheric). The downloaded datasets of 3-hour forced data were linearly interpolated to hourly resolution. All input data were reprojected to the same coordinate system.

Soil type and soil infiltration porosity in the top four layers (Figures 2c and 2d) from a 1 km resolution global soil map (Zhang et al., 2018) and the world soil database (http://www.fao.org/data/en/), the soil classification of the study area was mainly sand, loamy sand, sandy loam, loam, Silty clay loam, clay loam, clay with clay occupying 85% of the study area. Seven soil units were used to represent the top soil layer of ParFlow and CLM exchange (Table 1), and the vegetation type of the whole model domain was assumed C3 plants with leaf area index between 1.20 and 3.40.

The land use data (Figure 2b) for this study (2018-2021) were obtained from Esri_Land_Cover_10m using the 10m high-resolution land cover classification from Sentinel-2, resampling the map to a model grid resolution of 100m and then mapped the land-cover categories to the Common Land Model International Geosphere-Biosphere Programme (CLM IGBP) land cover categories (Table 2). For the general topography, DEM with a resolution of 12.5m measured by the ALOS (Advanced Land Observing Satellite) satellite were obtained from https://search.asf.alaska.edu/#/.

The algorithm and the terrain processing tool priority flow (R package) proposed by Condon et al (2019) to calculate the topographic slope in x and y directions (S_x and S_y) as input to the ParFlow slope flow simulation (Barnes et al., 2014; Barnes et al., 2018). The streams form naturally as surface water is routed by topography and the flow direction grid was adapted in the GRASS plugin of QGIS (Geographic Information System) (Yang et al., 2020). A parking lot test was conducted to check the accuracy of the drainage network, and the top boundary condition was set to rain on the domain intermittently for the parking lot test to further correcting the slope (Bhaskar, 2010).
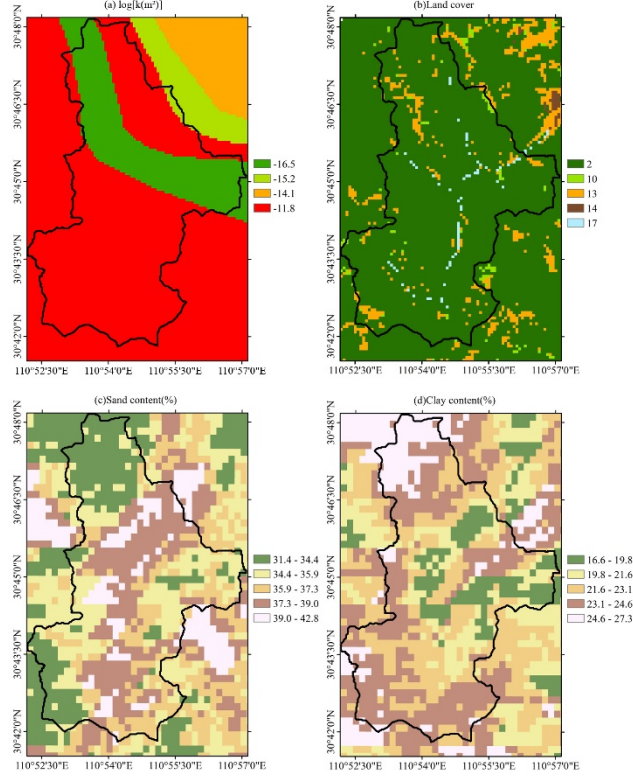
Figure 2. (a) logarithmic permeability (logk) of the deep aquifer (f) in the modeling domain; (b) Land cover; (c) Sand content of the surface soil; (d) Clay content of the surface soil.

Numbers 1-17 in the land cover subpanel correspond to surface types defined by the International Geosphere Biosphere Program (IGBP), and for details please refer to Table 2.

Table 1. Hydrogeological Properties Assigned to Model Domain

@ >p(- 10) * >p(- 10) * >p(- 10) * >p(- 10) * >p(- 10) * >p(- 10) * @
Hydrogeological unit & Depth

below land surface(m) & Layer thicknesses comprising unit (m) & Indicator

Units & Porosity & Permeability

(m/hr)
Soil & 0-4 & 0.2,0.3,0.5,0.5,2.5 & sand

loamy sand

sandy loam & 0.38

0.39

0.39 & 0.2691

0.0436

0.0158
& & & loam

Silty clay loam & 0.46

0.38 &

  0.0046

& & & clay loam & 0.44 & 0.0034
& & & clay & 0.46 & 0.0062
aquifer & 4-109 & 105 & f.s sedimentary

sil sedimentary

crystalline & 0.12

0.19

0.01 &

  0.02

  0.03

  0.04

& & & carbonate & 0.06 & 0.10

Table 2. Mapping of the Sixi Land Cover Class to Common Land Model International Geosphere Biosphere Programme (CLM IGBP) Land Cover Class

Sixi Land Cover Class	CLM IGBP Land Cover Class
Water	17 water bodies
Grass	10 Grasslands
Forest	2 evergreen broadleaf forests
Agriculture	14 cropland
Urban Building	13 urban and built-up lands
Bare soil	18 bare soil

3.7 Model boundary conditions and spin-up

Groundwater is the slowest moving part which start easily with a simplified system and get a stable water table before adding in land surface processes (Ajami et al., 2014; Seck et al., 2015). In this study, the free surface slope flow boundary condition is set for the land surface (z-upper), and the no-surface flow boundary condition, i.e., the zero-flux boundary condition, is used for the other boundaries (Maxwell & Miller, 2005; Rahman et al., 2016). The initial water level is set to 4 m below the surface, and the initial water level runs for a long time continuously without CLM with a constant at the land surface until the difference between outflow and recharge rates was less than 1 % of total water storage change. To ensure proper model equilibrium, the transient simulation with the fully coupled ParFlow.CLM was run for 2-3 years of repeated atmospheric forcing to provide an initial condition for the simulation in this study.

3.8 hydrogeology

The deep aquifer of the study area consists mainly of carbonate (strong water content), sil sedimentary (weak water content), crystalline (moderate water content), and impervious bed. Four hydrogeological units (Table 1) represent the subsurface layers of the study area. The porosity, hydraulic conductivity, and permeability (Figure 2a) refer to the GLobal HYdrogeology MaPS 2.0 (GL-HYMPS 2.0) (Huscroft et al., 2018; Shangguan et al., 2017; Gleeson et al., 2014; Gleeson et al., 2011; Zhang et al., 2018; Foster & Maxwell 2019). For the Manning coefficients, one can consider the scaling of parameters when using the coarsening grid models, the stream cells defined and assigned a typical stream Manning's n (0.035 s m$^{-1/3}$) after scaling and all other cells determined by vegetation (Schalge et al., 2019; Soltani et al., 2022).

3.9 The significance of EEMD

The EMD (empirical mode decomposition) is a method developed by Huang et al. (1998) is a new adaptive time-frequency localization analysis method that escapes the limitations of the Fourier transform. It decomposes a signal into a finite set of Intrinsic Mode Functions (IMFs) and residual series, with each IMF representing a scale of data variability, where the sum of the IMFs and the residual component represent the complete data (Wu & Huang, 2005, 2009; Almendra et al., 2022; Adarsh & Janga Reddy, 2019; Huang & Wu 2008). The process of extracting the Intrinsic Mode Functions (IMFs) from a time series (which is called as "sifting" process) consists the following steps:

1. The given function u (t), find all the maxima and minimal value points of this function.

2. Connect maxima points and minima points using suitable interpolation function (say, cubic spline) to construct an upper envelope of maxima value and a lower envelope of minima value.

3. The two upper and lower envelopes are averaged to obtain the mean m (t)

and calculate the new difference time series function h (t) = u (t)-m (t).

4. Replace the original function with the function h(t) and repeat steps 1 to 3, obtaining h_k (t) until h_k (t) becomes a zero-mean series, defining imf (t) = h_k (t).

Wu and Huang (2005) found that EMD is an effective filter to separate white noise, and derived the expressions for the relationship between the energy density and the average period of the IMF components from white noise (which are confirmed by the Monte Carlo method). The significance test of the ensemble empirical modal decomposition constructs a long artificial white-noise record as a reference, and decomposes the targeted noisy dataset and the reference white-noise data into IMFs. The energy distribution at a confidence level are calculated and the energy density of the IMFs and the spread function are compared if the energy lies between the upper and lower limits, one can say that the signal is "contaminated" with white noise, the IMFs that have their energy located above the upper bound and below the lower bound should be considered to the data are statiscally significant at that selected confidence level(Wu & Huang, 2004; Almendra et al., 2022; Sang et al., 2014).

3.10 Performance evaluation metrics

As a measure of average magnitude accuracy with an optimal value of 0, percent bias is given by

(4)

where S_i and O_i are simulated and observed values.

Spearman's rank correlation coefficient, or Spearman's :

(5)

Spearman's independently ranks the simulated and observed values, with bi in Eq. (9) being the difference in ranks for a given value i, and n is the number of values in the series. is less restrictive; it does not assume linearity and instead tests for monotonic correlation. The optimal value for is 1, and the cutoff for good performance is likely analogous to that of R^2, which varies in the literature but is generally around 0.6. (O'Neill et al., 2020)

The mean absolute error (MAE):

(6)

The root mean square error ($RMSE$):

(7)

The Nash-Sutcliffe Efficiency (NSE):

(8)

The correlation coefficient (r):

11

(9)

4 Result and Discussion

4.1 The evaluation of coarsening DEM

The NN, MJ, and HD coarsening techniques were evaluated by comparing the flow channels recovered from the coarsened digital elevation model to the high resolution grid digital elevation model and by comparing the depression-filled heights in the coarsened grid digital model with the original elevations.
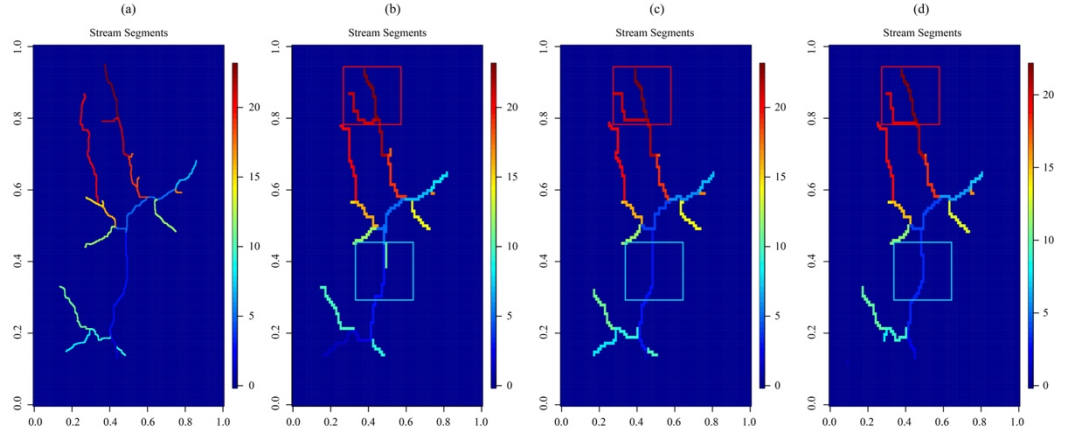

Figure 3. The extracted surface flow paths from 10m high-resolution and HD, MJ, NN coarsening grid digital elevation models.

(a) 10 m grid digital elevation model and extracted surface flow path used as a reference. (b) 100m grid digital elevation model obtained from hydrography-driven(HD) coarsening plus depression-filling and extracted surface flow path. (c) 100m grid digital elevation model obtained from MJ coarsening plus depression-filling and extracted surface flow path. (d) 100m grid digital elevation model obtained from NN coarsening plus depression-filling and extracted surface flow path.

Comparing the surface flow paths extracted from the high resolution 10m grid digital elevation model of the study area, the highest-order path (red line) of the HD extracted curve river channel according to topography and retains the basic topographic information about the mainstream channel (blue line) observed in the coarse grid cell (Figure 3b). NN accurately describes the topographic information about valley and channel thalwegs observed in high-resolution topographic data (Figure 3c). When high-resolution topographic data using MJ coarsening, loss the information on topography about the partial of tributaries (red line) and the mainstream channel (blue line) (Figure 3d). The topographic information is easily lost when high-resolution topographic data describing a trough area are coarsened by using standard NN coarsening and MJ coarsening.
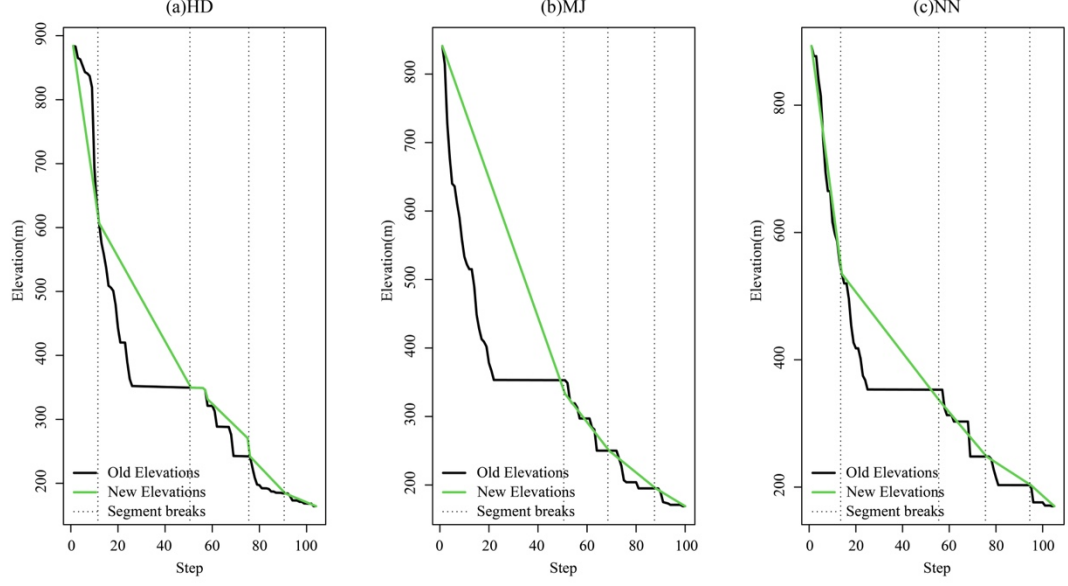
Figure 4. Comparison of the drainage system mainstream elevations observed, in high-resolution topographic data and in digital elevation models obtained from nearest neighbor(NN), majority method (MJ), and hydrography-driven (HD) coarsening.

(a) New elevation of the mainstream channel after depression-filling from a hydrography-driven (HD) coarsening of the 100m grid digital versus the original elevation (b) New elevation of the mainstream channel after depression-filling from a majority (MJ) coarsening of the 100m grid digital versus the original elevation. (c) New elevation of the mainstream channel after depression-filling from a nearest neighbor (NN) of the 100m grid digital versus the original elevation.

The MJ coarsening strategy produces local artifacts and abnormal depression-filling in upstream areas (Figure 4b), filling depression with a straight line to the upstream elevation instead of filling depression close to elevation, while HD and NN after depression-filling are significantly closer to the elevation of the upstream area observed in the high resolution topographic data (Figures 4a and 4c). The results reported in Figure 4 reveal the ability of the HD coarsening strategy retain the terrain orientation in the high-resolution topographic data and the information regarding estuary elevation and reduce impact of depression-filling.

In overall, the greater ability of the HD coarsening strategy to preserve the information content of high-resolution topographic data as compared to the MJ and NN coarsening strategies, the HD coarsening strategy maintains the deep contours observed in the high-resolution terrain data and minimizes the effects of depression filling. The elevation used in the HD coarsening is hydrographically

13

more significant than the elevation used in the MJ and NN coarsening strategies as it provides a better description of the profiles of surface flow paths with direct implications on the description of land surface topography due to the reduction of the impact of depression-filling.

4.2 Discharge

In many karst systems worldwide, numerous karst features facilitate the exchange of water between the surface, the vadose zone and porous aquifers (Bailly-Comte et al. 2008). These interactions play an important role in the surface water and groundwater cycle processes. Karst trough areas have complex topographic features, and therefore the slope of the model inputs with direct implications on the flow estimation from the model simulations. The choosing of the coarsening method with a remarkably better ability to preserve the information content of high-resolution topographic data is essential for an integrated hydrological model to calculate hydrological fluxes.

In this study, the different coarsening strategy simulated water balance component (Streamflow and Evapotranspiration) is generally judged to be excellent for this purpose with the following measures: $MAE < 0.6$, > 0.6, $NSE > 0.7$, or $PBIAS < 20\%$.

Figure 5 demonstrate the ability of ParFlow.CLM simulated hourly overland flow for 2018 year using different coarsening methods at the outlet. The HD, MJ, and NN coarsening strategies for Spearman's are 0.85, 0.77 and 0.82, while the same for NSE are 0.71, 0.59 and 0.66, $PBIAS$ are -5.14%, -10.15% and -2.35%, MAE are 0.42, 0.60 and 0.49 respectively (Figure 5). The performance of streamflow simulation varies widely across the coarsening strategies. For instance, HD coarsening strategy also appropriately simulate observed flows perform with $MAE < 0.5$, > 0.5 and $PBIAS < 10\%$, $NSE > 0.7$, with the correlation coefficient (r) > 0.8, meeting performance criterias (Figure 5b). While the results of the simulated streamflow by the NN coarsening method perform with $MAE < 0.5$, > 0.5 and $PBIAS < 10\%$, $NSE > 0.6$, $PBIAS$ = -2.35% showing that the simulation tends to overestimate the observed flows (Figure 5a). Conversely, the results of the simulated streamflow by the MJ coarsening strategy shows poor timing performance (of 0.32) and higher overall bias (Figure 5c). The results of the simulated streamflow by the NN coarsening method perform with $MAE < 0.6$, > 0.3 and $PBIAS < 20\%$, $NSE > 0.5$, $r > 0.7$, $PBIAS$ = -10.15%, and NSE = 0.59 not fit the performance criteria and struggles to capture low flows, indicating that the MJ coarsening strategy is certainly the coarsening strategy with the worst streamflow simulation performance. Overall, in the case of streamflow simulation, HD, MJ and NN coarsening methods all overestimate the observed streamflow, HD coarsening method perform slightly better than NN coarsening method. NN and HD coarsening offers a remarkably better ability than the MJ coarsening to simulate streamflow at the outlet.
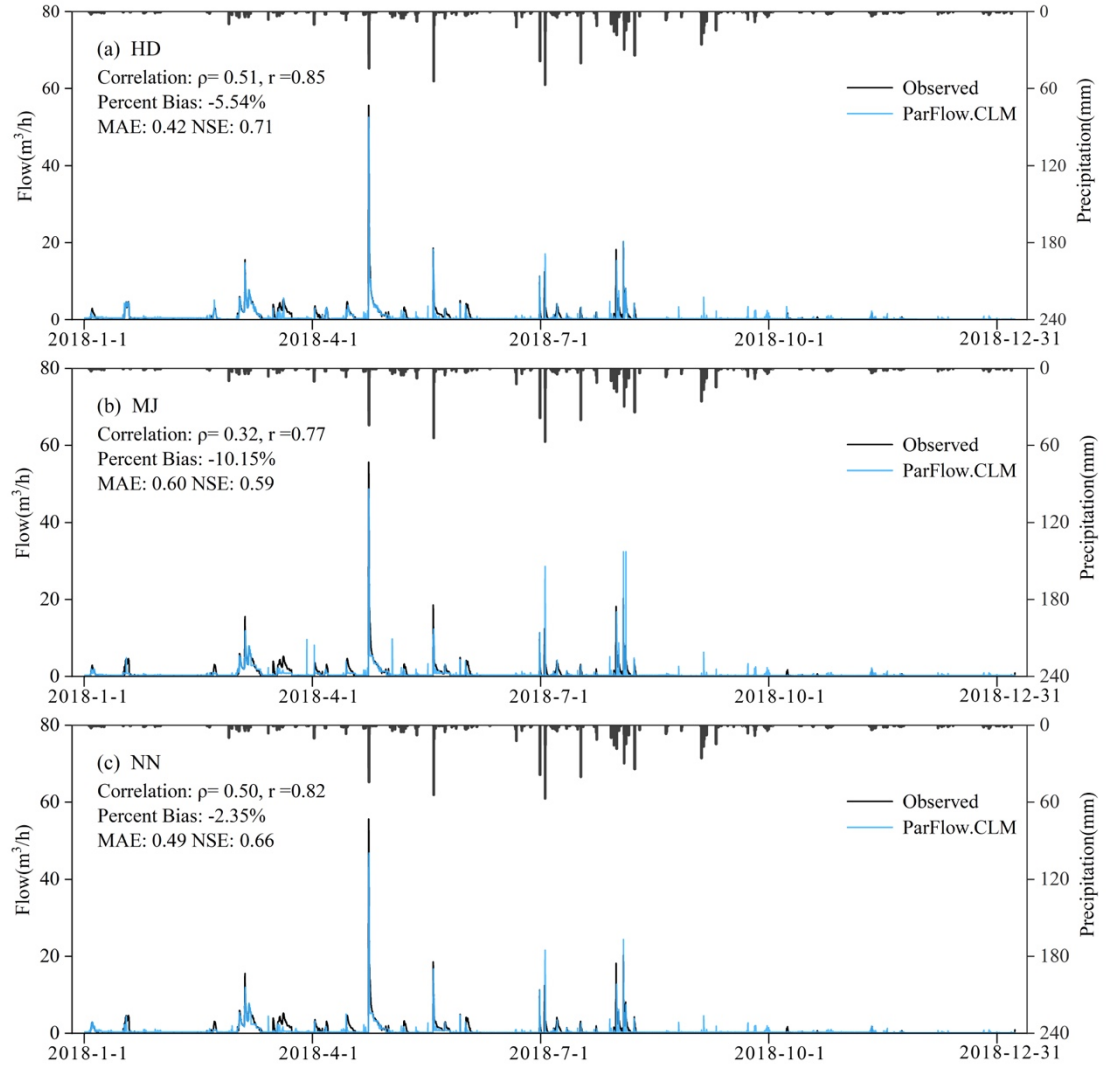
Figure 5. Comparison of hourly observed flow and simulated flow by three coarsening methods of HD, MJ and NN at the outlet of the study area.

4.3 Evapotranspiration

Figure 6 compares the simulated daily ET using different coarsening methods for 2021 year with the observed evapotranspiration. The simulated ET results of HD coarsening strategy perform with Spearman's ρ are 0.61, the correlation coefficient (*r*) are 0.71, the *MAE* are 0.46 and *PBIAS* are 12.70%, fitting the performance criteria for each indicator and showing good agreement with the observed values in the summer, autumn and winter seasons (6-12) (Figure 6a).

15

The simulated ET results of MJ coarsening strategy perform with Spearman's are 0.37, the correlation coefficient (r) are 0.43, the *MAE* are 0.65 and *PBIAS* are 34.15%, the simulated ET results of NN showed perform with Spearman's are 0.39, the correlation coefficient (r) are 0.41, the *MAE* are 0.58 and *PBIAS* are 33.62% (Figure 6b). The evapotranspiration simulation curves for MJ and NN coarsening methods did not show peaks consistent with observed values in the case of heavy rainfall, and simulated values of both coarsening methods underestimated observed value in summer and autumn season and overestimated observed values in winter season. While The NN coarsening method revealed a prominent ability to simulate evapotranspiration in spring autumn (Figure 6c). The error in the wet period is clearly lower than the error in the dry period. The different performance metrics indicate that the HD coarsening method perform better than NN and MJ coarsening method and NN coarsening method perform slightly better than MJ coarsening method.

The results indicate that there is a nonlinear and nonsystematic influence of slope at the same meteorological forcing conditions on the evapotranspiration simulation. When using coarse resolution hydrological models, any depression within the grid cells can lead the magnitude of the slope resulting in locally to large underestimation of evapotranspiration. The gentle slope cases are generally wetter locally (i.e., highest ET, higher runoff, and hydraulic pressure head) (Leonarduzzi et al., 2021). HD coarsening method overestimates evaporation during the wet season (when rainfall is high), while MJ and NN coarsening method underestimates evapotranspiration during the wet season and does not reach the peak of ET during periods of high rainfall. 4.1 indicates that the loss of terrain information when using the MJ and NN coarsening method leads to the slope of the grid cells being high, resulting in an underestimation of the simulated peak of ET for the MJ and NN coarsening method. The value of the simulated ET by MJ and NN coarsening method has a much weaker consistency with the observed ET than HD coarsening method.
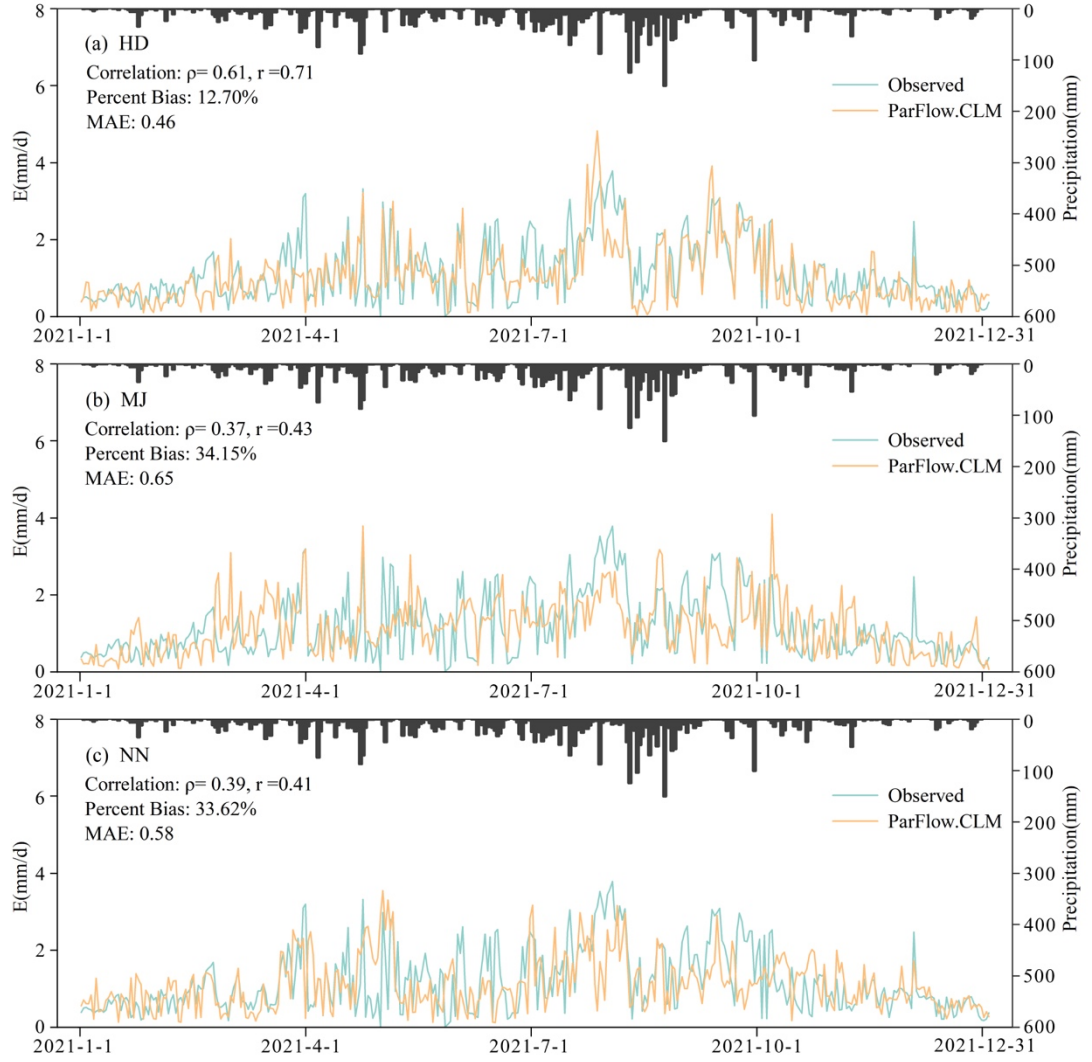
Figure 6. Comparison of daily observed evapotranspiration and simulated by three coarsening methods of HD, MJ and NN.

4.4 Soil moisture

Figure 7 illustrates the temporal variation curves of the simulated hourly soil moisture and observed values using different coarsening methods. The results show that the soil moisture at 20 cm depth simulated by HD, MJ and NN coarsening methods all underestimate the observed at 20 cm (HD: $PBIAS = 0.031\%$, MJ: $PBIAS = 0.024\%$, NN: $PBIAS = 0.018\%$) (Figure 7a and Table 3). The simulated soil moisture at 20cm is in good consistency with the observed actual

soil moisture performed with the HD coarsening method, has a high correlation coefficient (0.608; maximum), high spearman coefficient (= 0.593), small bias ($PBIAS = 0.031\%$), and small MAE (0.037; minimum) (Table 3). The simulated soil moisture at the 20cm depth curve of HD coarsening method generally agrees with the observed curve in the autumn season (8-10 in 2021) (Figure 7a and Table 3). However, the simulation performance of the HD coarsening method is weaker in the case of simulating soil moisture at 50 cm depth, with the correlation coefficient of r (0.559) and small Spearman's (0.549), but was able to resemble well soil moisture in summer season (Figure 7a and Table 3). The HD coarsening method model simulations tend to underestimate soil moisture at 50 cm depth, particularly during winter conditions. In general, the hourly soil moisture is predicted by the ParFlow.CLM using HD coarsening method at 20cm and 50cm depths agree with the observed SM data relatively better in the summer and autumn seasons than in the spring and winter seasons.

MJ coarsening method was not able to resemble well soil moisture at the 20 cm depth in the spring season (1-3 in 2022). The performance evaluation metrics indicate a poor model performance for soil moisture simulation at 20cm depth for the overall model of the MJ coarsening method, with small correlation coefficient r (0.575; minimum), small Spearman's (0.542; minimum), and MAE (0.041; medium) (Figure 7b and Table 3). The model performance improved at 50 cm depth. It was able to resemble well soil moisture in summer-autumn (4-6 in 2021), but the overall model still underestimated the soil moisture at 50 cm depth ($PBIAS = 0.012\%$), with a high Spearman coefficient (0.727) and a high correlation coefficient r (0.693) (Table 3). MJ coarsening method could resemble better soil moisture at the 50 cm depth during the summer season and dry period (8-9) for the 2021 year (Figure 7b).

The simulated values of NN at 20 cm depth tend to be lower, especially during the autumn rainy season (i.e. July). Both overestimation (e.g. October 2021) and underestimation (e.g. April-July 2021) of soil water moisture occurred (Figure 7c and Table 3). The NN coarsening method simulated soil moisture at 20cm depth with MAE at 0.042, Spearman's at 0.595, and the correlation coefficient (r) at 0.606. At 50 cm depth the percent bias of simulated soil moisture was reduced to -0.002%, with MAE are 0.022, Spearman's coefficient being 0.565, and the correlation coefficient (r) are 0.563 (Table 3). The overall model performance of the NN coarsening method was moderate in MJ and HD coarsening methods, this is also supported by performance indices listed in Table 3.

The results clearly show that the HD coarsening method performs better than NN and MJ coarsening method for the SM simulation at the 20cm depth, and MJ coarsening method performs better than NN and HD coarsening method for the SM simulation at the 50cm depth. The overall model performance of the NN coarsening method was moderate in MJ and HD coarsening method for the SM simulation.
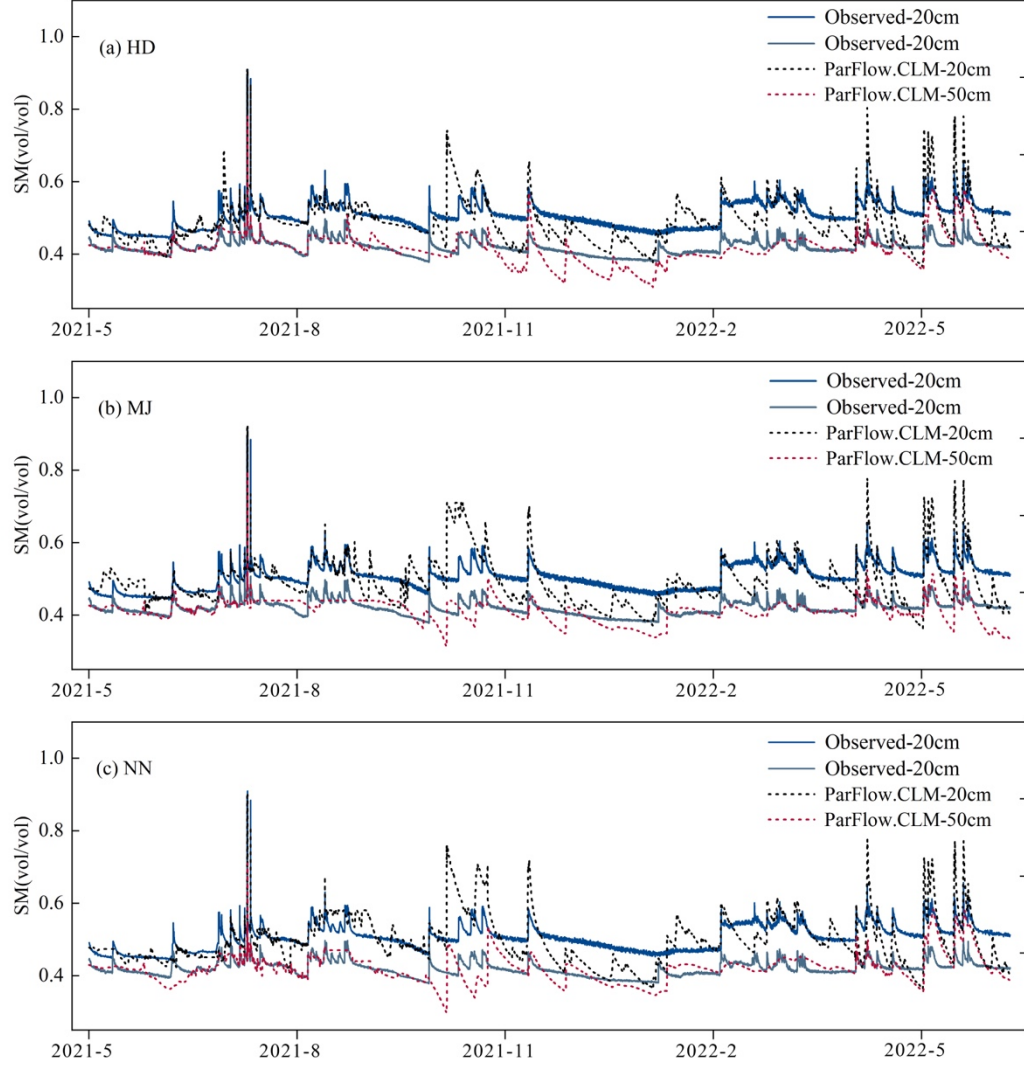
Figure 7. Comparison of hourly observed soil moisture at 20 cm depth and 50 cm depth and simulated by three coarsening methods in HD, MJ and NN.

The simulations provide information on the potential errors associated with differences in coarsening methods when coarsening high-resolution digital elevation models into coarse-grid digital elevation models, which can affect surface soil moisture when regional hydrological models and coarse-resolution grid models are used to calculate hydrological fluxes. At coarse grid scales, due to grid heterogeneities, the region of land classification becomes more significant at coarse grid scales and leading to overestimation or underestimation of soil moisture and loss of topographic information at coarser scales, leading to gentle topog-

19

raphy, with lower evapotranspiration and lower streamflow, and overestimation of surface soil moisture.

For a better understanding of how soil moisture is influenced by topographic configuration and soil geometry(Baroni et al., 2019), the variation in the spatially distributed simulated infiltration by three different coarsening method on 2 January to 6 January 2021 is depicted in Figure 8. The model of different coarsening method simulations showed similar mean infiltration, but the structure differed remarkably in the spatial distribution. At the equivalent meteorological forcing conditions, it can be shown that the distribution of infiltration is not correlated to the precipitation distribution but rather to soil properties and land use (cf. Figures 8 and 2), the smaller-scale hydrological fluxes spatial structures simulated by ParFlow.CLM are strongly related with the river network and topography. Different coarsening methods lead to significant differences in the spatial distribution of infiltration, with the simulation of infiltration spatial distribution for HD coarsening method being the most realistic (Figures 8a and 2a).
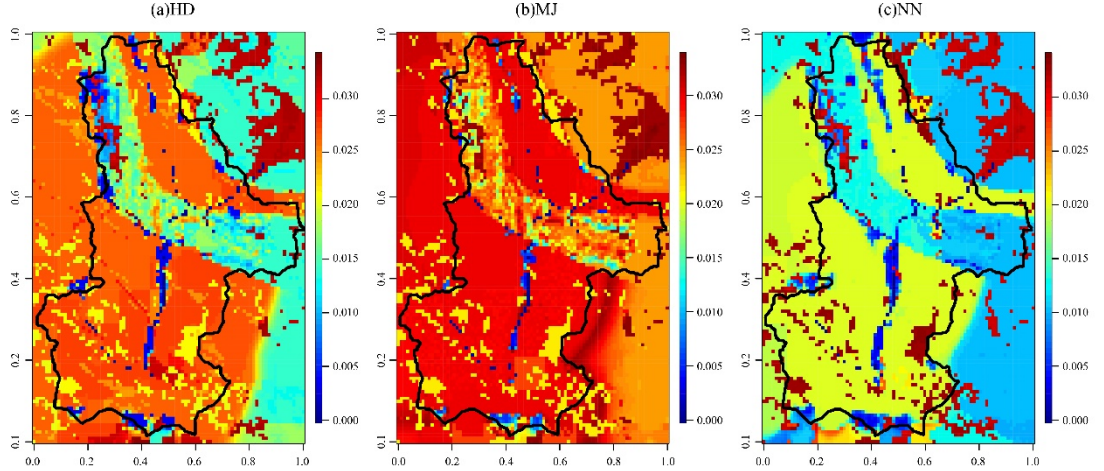

Figure 8. The spatially distributed simulated hourly mean soil infiltration (mm H2O/s) by three coarsening methods of HD, MJ and NN at the identical meteorological forcing.

Figure 9 shows the EEMD significance test of the simulated soil moisture at the 20cm and 50cm depth of the three coarsening methods. The blue and red curves represent the 95% and 99% significance range; values outside this range are statistically significant at 95% and 99%, respectively.

In the case of simulating soil moisture at the 20cm depth, the energy of IMF 1-10 of three coarsening methods all passed the 95% significance range (Figures 9a-9c). In the case of simulating soil moisture at the 50cm depth, the energy of IMF 1-10 of HD and MJ coarsening method passed the 95% significance range

(Figures 9d and 9e). For NN coarsening method, the components of IMFs of evapotranspiration simulation passed 95% significance test, except for IMF3, IMF4 and IMF5 (Figure 9f). From the regression coefficient matrix of soil moisture simulation at the 20cm depth for the three coarsening methods (Table 4), it is noticed that the components of IMFs of three coarsening methods passed the 95% significance test. The components of SM simulation at 20cm depth of HD and MJ coarsening method positively influence their respective modes. For NN coarsening method, except for IMF4, the components of IMFs have a positive influence on the modes. In the case of the SM, simulation at 50cm depth (Table 5), the components of IMFs of HD coarsening method positively influence the modes, except for IMF7. The components of IMFs of the MJ coarsening method all positively influence the modes. For the NN coarsening method, the coefficients of IMF1 and IMF2 negatively influence the modes.

The results indicate that the simulated SM results of the three coarsening methods are all statistically significant.
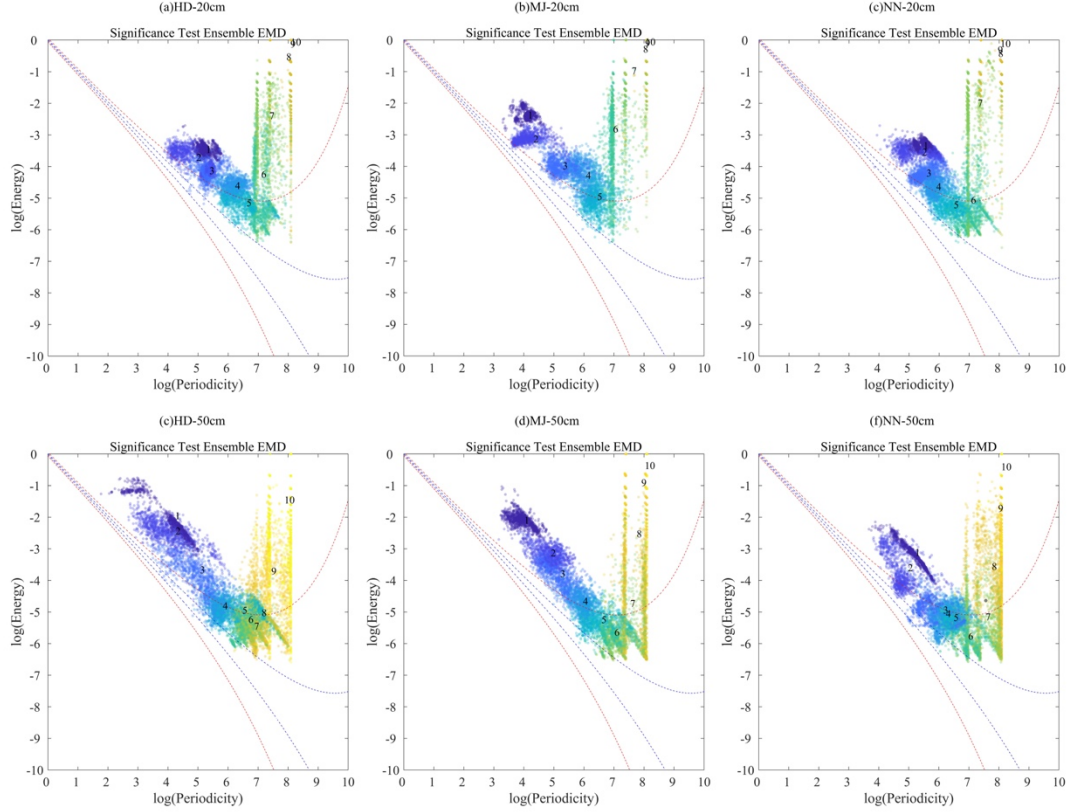

Figure 9. The EEMD significance test result of simulated soil moisture at 20 cm depth and 50 cm depth for three coarsening methods in HD, MJ and NN.

Table 3. Performance evaluation metics(PEM) of different models for soil moisture simulations

Methods	PEM	SM(20cm)	SM(50cm)
HD	MAE	0.037	0.019
	PBIAS	0.031	0.021
	r	0.608	0.559
	Spearman's	0.593	0.549
	RMSE	0.050	0.027
MJ	MAE	0.041	0.022
	PBIAS	0.024	0.012
	r	0.575	0.693
	Spearman's	0.542	0.727
	RMSE	0.055	0.031
NN	MAE	0.042	0.022
	PBIAS	0.018	-0.002
	r	0.606	0.563
	Spearman's	0.595	0.565
	RMSE	0.055	0.033

Table 4. Regression coefficient matrix for the IMFs of simulated soil moisture at 20 cm depth of HD, MJ, and NN coarsening methods.

Methods	Mode number	Regression coefficients for mode number	P>t
HD	IMF1	0.397	0.000
	IMF2	0.353	0.000
	IMF3	0.201	0.000
	IMF4	0.186	0.000
	IMF5	0.601	0.000
	IMF6	0.305	0.000
MJ	IMF1	0.498	0.000
	IMF2	0.513	0.000
	IMF3	0.392	0.000
	IMF4	0.395	0.000
	IMF5	0.189	0.000
	IMF6	0.311	0.000
	IMF7	1.183	0.000
NN	IMF1	0.266	0.000
	IMF2	0.279	0.000
	IMF3	0.188	0.000
	IMF4	-0.181	0.000
	IMF5	0.746	0.000
	IMF6	0.394	0.000

Table 5. Regression coefficient matrix for the IMFs of simulated soil moisture at 50 cm depth of HD, MJ, and NN coarsening methods.

Methods	Mode number	Regression coefficients for mode number	P>t
HD	IMF1	0.165	0.000
	IMF2	0.188	0.000
	IMF3	0.366	0.000
	IMF4	0.373	0.000
	IMF5	0.388	0.000
	IMF6	0.646	0.000
	IMF7	-3.045	0.000
MJ	IMF1	0.498	0.000
	IMF2	0.513	0.000
	IMF3	0.392	0.000
	IMF4	0.395	0.000
	IMF5	0.189	0.000
	IMF6	0.311	0.000
	IMF7	1.183	0.000
NN	IMF1	-0.027	0.375
	IMF2	-0.019	0.231
	IMF3	0.156	0.000
	IMF4	0.289	0.000
	IMF5	0.483	0.000
	IMF6	0.213	0.000
	IMF7	0.309	0.000

4.5 Latent heat fluxes and top soil temperatures

The difference in hourly top soil temperatures simulated by HD, MJ and NN coarsening methods for 2021 year relative to observed value in the ERA5 is depicted in Figure 10. The HD coarsening strategies for Spearman's =0.95, *PBIAS*=0.66%, R^2=0.82, *NSE*=0.895, the MJ coarsening strategies for Spearman's =0.94, *PBIAS*=0.52%, R^2=0.85, *NSE*=0.892, the MJ coarsening strategies for Spearman's =0.94, *PBIAS*=0.63%, R^2=0.82, *NSE*=0.891 (Figures 10a-10c). The boxplot and each performance metrics of the simulated and observed top soil temperature value indicate that HD coarsening method perform slightly better than MJ coarsening method, MJ coarsening method perform slightly better than NN coarsening method, and there are minor differences between the simulations for HD, MJ and NN coarsening method. The results reveal that the top soil temperature simulated by ParFlow.CLM is not sensitive to slope.

Boxplot of the simulated and observed latent heat fluxes for the 2021 year demonstrate that the simulated latent heat fluxes by HD, MJ, and NN coarsening method has weaker consistency with observed value performed with more anomalies, and the median (green line) differs significantly from observations

for the same meteorological forcing (Figures 11a-11c). The results indicate a poor model performance for latent heat fluxes simulation for all models. This situation may be due to the ERA5 hourly meteorological forcing being bilinear interpolated in the study area; Thus, the deviations of precipitation, evaporation, wind speed, humidity, and radiation can be derived from the data processing or scaling of ERA5, resulting in model-calculated latent heat fluxes that differ significantly from the observed values. Major biases exist in preprocessing of ERA5 meteorological forcing and topography, latent heat fluxes, soil moisture, evapotranspiration, and streamflow are sensitive to errors in drainage area, topographic region, and precipitation or temperature bias.
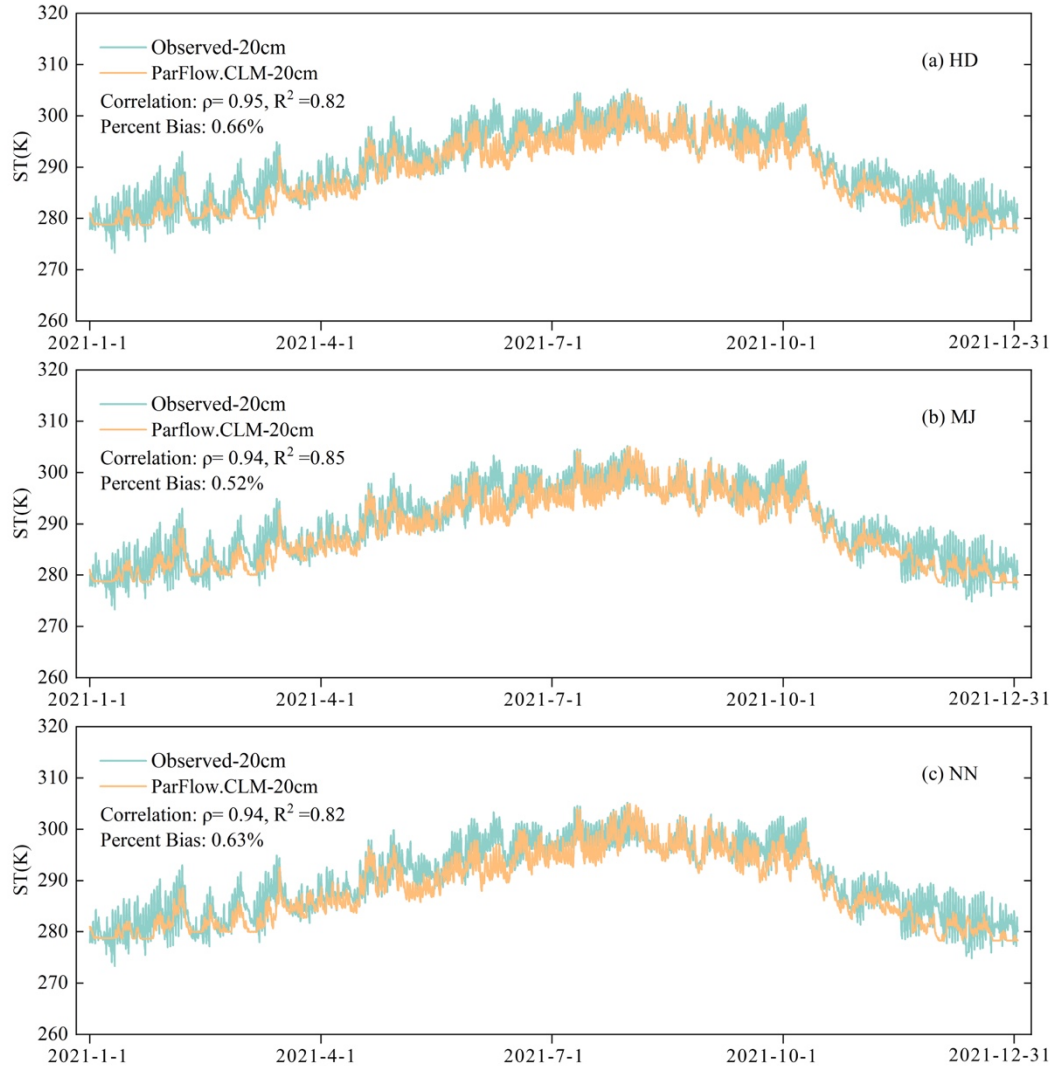
Figure 10. Comparison of hourly observed soil temperature at 20 cm depth and simulated by three coarsening methods of HD, MJ and NN.
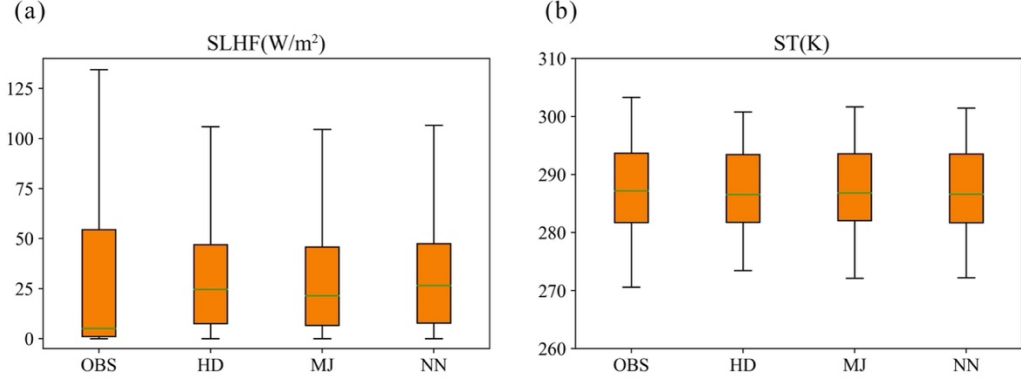

(a)

SLHF(W/m²)

(b)

ST(K)

Figure 11. The box plot of soil temperature(ST) at 20 cm depth and latent(LE) heat flux simulated and observed for three coarsening methods in HD, MJ and NN.

5 Conclusion

In karst trough areas with complex topographic terrain, the slope is important in affecting the resulting hydrologic fluxes (discharge, ET, soil moisture, soil temperature etc.) simulated by an integrated hydrologic model. Considering that slope would affect the accuracy of hydrologic processes simulation, this work provides an option for the coarsening method in the application of hydrologic modeling. In this study, the numerical experiment based on the integrated hydrological model ParFlow-Common Land Model (ParFlow.CLM) was conducted to quantify the impact of different grid coarsening methods on the prediction results. The main findings are:

1. At the same meteorological forcing, trends in ET, infiltration, the 20cm and 50cm soil thickness moisture are most sensitive to slope, and the top soil temperature are less sensitive to the slope.

2. The combined *MAE*, *NSE*, *r*, *R²*, *PBIAS*, Spearman coefficient, and EEMD significance test demonstrated that HD coarsening method performs slightly better in the case of streamflow simulation case NN coarsening method. HD and NN coarsening offer a remarkably better ability than the MJ coarsening to simulate streamflow at the outlet. The value of the simulated ET by MJ and NN coarsening method has a much weaker consistency with the observed ET than HD coarsening method; the performance of NN coarsening method was better than the MJ coarsening method. In the case of SM simulation, the overall model performance of the NN coarsening method was moderate in MJ and HD coarsening methods. The accuracy of HD coarsening method simulation higher

than MJ coarsening method in the case of 20cm SM simulation. Oppositely, the accuracy of MJ coarsening method higher than HD coarsening method in the case of 50cm SM simulation. Different coarsening methods lead to significant differences in the spatial distribution of infiltration, with the simulation of spatial infiltration distribution for the HD coarsening method being the most realistic. For topsoil temperature, the R^2 value of HD, MJ, and NN coarsening methods exceeded 0.9, and HD coarsening method's simulation accuracy was slightly better than MJ and NN coarsening methods. Poor model performance for latent heat fluxes simulation for all model.

3. Concerning extracted surface flow paths, the drainage system mainstream of HD extracts the curved river channel according to the topography and retains the essential information about the highest-order path observed within the coarse grid cell. The topographic information is easily lost when high-resolution topographic data describing a trough area is coarsened by using standard NN coarsening and MJ coarsening.

As a result, the HD coarsening is hydrographically more significant than NN and MJ coarsening, as it provides a better description of the surface flow path that is more closely to the high-resolution topography and reduces the effects of depression-filling. The accurate description of the channel network and topographic information are critical for calculating hydrological fluxes (soil water moisture, streamflow and evapotranspiration) with an integrated model and exploring the hydrological interactions between the hillslope and channel network. The HD coarsening method is advocated for hydrological events where ParFlow.CLM uses coarse grid resolution to simulate hydrological processes requiring detailed descriptions of the topography and river channel grid.

Acknowledgements

References

Adarsh, S., & Janga Reddy, M. (2019). Evaluation of trends and predictability of short-term droughts in three meteorological subdivisions of India using multivariate EMD-based hybrid modelling. *Hydrological Processes*, 33(1), 130-143. https://doi.org/10.1002/hyp.13316

Ajami, H., McCabe, M. F., Evans, J. P., & Stisen, S. (2014). Assessing the impact of model spin-up on surface water-groundwater interactions using an integrated hydrologic model. *Water Resources Research*, 50, 2636-2656. https://doi.org/10.1002/2013WR014258

Almendra-Martín, L., Martínez-Fernández, J., Piles, M., González-Zamora, Á., Benito-Verdugo, P., & Gaona, J. (2022). Analysis of soil moisture trends in Europe using rank-based and empirical decomposition approaches. *Global and Planetary Change*, 215, 103868. https://doi.org/10.1016/j.gloplacha.2022.103868

Ashby, S. F., & Falgout, R. D. (1996). A parallel multigrid preconditioned conjugate gradient algorithm for groundwater flow simulations. *Nuclear Science and Engineering*, 124,145-159. https://doi.org/10.13182/NSE96-A24230

Bailly-Comte, V., Jourde, H., Roesch, A., Pistre, S., & Batiot-Guilhe, C. (2008). Time series analyses for Karst/River interactions assessment: Case of the Coulazou river (southern France), *Journal of Hydrology*, 349(1-2), 98-114. https://doi.org/10.1016/j.jhydrol.2007.10.028.

Barnes, M. L., Welty, C., & Miller, A. J. (2018). Impacts of development pattern on urban groundwater flow regime. *Water Resources Research*, 54(8), 5198-5212. https://doi.org/10.1029/2017WR022146

Barnes, R., Lehman, C., & Mulla, D. (2014). Priority-flood, an optimal depression-filling and watershed-labeling algorithm for digital elevation models. *Computers & Geosciences*, 62, 117-127. https://doi.org/10.1016/j.cageo.2013.04.024

Baroni, G., Schalge, B., Rakovec, O., Kumar, R., Schüler, L., Samaniego, L., et al. (2019). A comprehensive distributed hydrological modeling intercomparison to support process representation and data collection strategies. *Water Resources Research*, 55, 990-010. https://doi.org/10.1029/2018WR023941

Bhaskar, A. (2010). Getting started with ParFlow: Dead Run, Baltimore, Maryland example. UMBC/CUERE Technical Report 2010/002. University of Maryland, Baltimore County, Center for Urban Environmental Research and Education, Baltimore, MD. Retrieved from University of Maryland, Baltimore County

Condon, L. E., & Maxwell, R. M. (2019). Modified priority flood and global slope enforcement algorithm for topographic processing in physically based hydrologic modeling applications. *Computers and Geosciences*, 126, 73-83. https://doi.org/10.1016/j.cageo.2019.01.020

Condon, L. E., & Maxwell, R. M. (2014a). Feedbacks between managed irrigation and water availability: Diagnosing temporal and spatial patterns using an integrated hydrologic model. *Water Resources Research*, 50, 2600-2616, https://doi.org/10.1002/2013WR014868

Condon, L. E., & Maxwell, R. M. (2014b). Groundwater-fed irrigation impacts spatially distributed temporal scaling behavior of the natural system: A spatio-temporal framework for understanding water management impacts.

Environmental Research Letters, 9(3), 034009.https://doi.org/10.1088/1748-9326/9/3/034009

Condon, L. E., & Maxwell, R. M. (2015). Evaluating the relationship between topography and groundwater using outputs from a continental-scale integrated hydrology model. *Water Resources Research*, 51(8):6602-6621. https://doi.org/10.1002/2014WR016774

Clapp, R. B., & Hornberger G. M. (1978). Empirical equations for some soil hydraulic properties. *Water Resources Research*, 14(4) , 601-604. https://doi.org/10.1029/WR014i004p00601.

Dai, Y., Zeng, X., Dickinson, R. E., Baker, I., Bonan, G. B., Bosilovich, M. G., et al. (2003). The common land model. *The Bulletin of the American Meteorological Society*, 84(8), 1013-1023. https://doi.org/10.1175/BAMS-84-8-1013

De Bartolo, S., Dell'accio, F., Frandina, G., Moretti, G., Orlandini, S., & Veltri, M. (2016). Relation between grid, channel, and Peano networks in high-resolution digital elevation models. *Water Resources Research*, 52, 3527-3546. https://doi.org/10.1002/2015WR018076

Foster, L.M., & Maxwell, R. M. (2019). Sensitivity analysis of hydraulic conductivity and Manning's n parameters lead to new method to scale effective hydraulic conductivity across model resolutions. *Hydrological Processes*, 33, 332-349. https://doi.org/10.1002/hyp.13327

Gallant, J.C., & Hutchinson, M. F. (2011). A differential equation for specific catchment area. *Water Resources Research*, 47(5). https://doi.org/10.1029/2009WR008540

Gleeson, T., Moosdorf, N., Hartmann, J., & van Beek, L. P. H. (2014). A glimpse beneath earth's surface: GLobal HYdrogeology MaPS(GLHYMPS) of permeability and porosity. Geophysical Research Letters, 41, 3891-3898. https://doi.org/10.1002/2014GL059856

Gleeson, T., Smith, L., Moosdorf, N., Hartmann, J., Durr, H. H., Manning, A. H., et al. (2011). Mapping permeability over the surface of the Earth. Geophysical Research Letters, 38, L02401. https://doi.org/10.1029/2010GL045565

Hein, A., Condon, L., & Maxwell, R. (2019). Evaluating the relative importance of precipitation, temperature and land-cover change in the hydrologic response to extreme meteorological drought conditions over the North American High Plains. *Hydrology and Earth System Sciences*, 23(4), 1931-1950. https://doi.org/10.5194/hess-23-1931-2019

Hester, E. T., & Doyle, M. W. (2008a). In-stream geomorphic structures as drivers of hyporheic exchange. *Water Resources Research*, 44(3). https://doi.org/10.1029/2006WR005810

Hester, E. T., & Doyle, M. W. (2008b). In-stream geomorphic structures as drivers of hyporheic exchange. *Water Resources Research*, 44(3).

https://doi.org/10.1029/2006WR005810

Huang, N., & Wu, Z. (2008). A review on Hilbert-Huang transform: Method and its applications to geophysical studies. *Reviews of Geophysics*, 46(2), n/a-n/a. https://doi.org/10.1029/2007RG000228

Huang, N. E., Shen, Z., Long, S. R., Wu, M. C., Shih, H. H., Zheng, Q., et al. (1998). The empirical mode decomposition and the Hilbert spectrum for nonlinear and non-stationary time series analysis. Proceedings of the Royal Society of London. *Series A, Mathematical and Physical Sciences*, 454 (1971), 903-995. https://doi.org/10.1098/rspa.1998.0193

Huscroft, J., Gleeson, T., Hartmann, J., & Börker, J. (2018). Compiling and mapping global permeability of the unconsolidated and consolidated Earth: GLobal HYdrogeology MaPS 2.0 (GLHYMPS 2.0). *Geophysical Research Letters*, 45, 1897-1904. https://doi.org/10.1002/2017GL075860

Jencso, K. G., Mcglynn, B. L., Gooseff, M. N., Wondzell, S. M., Bencala, K. E., & Marshall, L. A. (2009). Hydrologic connectivity between landscapes and streams: Transferring reach- and plot-scale understanding to the catchment scale. *Water Resources Research*, 45(4). https://doi.org/10.1029/2008WR007225

Jones, J. E., & Woodward, C. S. (2001). Newton-krylov-multigrid solvers for large-scale, highly heterogeneous, variably saturated flow problems. *Advances in Water Resources*, 24, 763-774. https://doi.org/10.1016/S0309-1708(00)00075-0

Kenny, F., Matthews, B., & Todd, K. (2008). Routing overland flow through sinks and flats in interpolated raster terrain surfaces. *Computers and Geosciences*, 34(11), 1417-1430. https://doi.org/10.1016/j.cageo.2008.02.019

Kirchner, J. W. (2006). Getting the right answers for the right reasons, linking measurements, analyses, and models to advance the science of hydrology. *Water Resources Research*, 42(3). https://doi.org/10.1029/2005WR004362

Kollet, S.J., & Maxwell, R. M. (2006). Integrated surface–groundwater flow modeling, A free-surface overland flow boundary condition in a parallel groundwater flow model. *Advances in Water Resources*, 29(7), 945-958. https://doi.org/10.1016/j.advwatres.2005.08.006

Leonarduzzi, E., Maxwell, R. M., Mirus, B. B., & Molnar, P. (2021). Numerical analysis of the effect of subgrid variability in a physically based hydrological model on runoff, soil moisture, and slope stability. *Water Resources Research*, 57, e2020WR027326. https://doi.org/10.1029/2020WR027326

Lindsay, J. B. (2016). The practice of DEM stream burning revisited. *Earth Surface Processes and Landforms*, 41(5), 658-668. https://doi.org/10.1002/esp.3888

Maxwell, R. M. (2013). A terrain-following grid transform and preconditioner for parallel, large-scale, integrated hydrologic modeling. *Advances in Water Resources*, 53, 109-117. https://doi.org/10.1016/j.advwatres.2012.10.001

Maxwell, R. M., Condon, L. E., & Kollet, S. J. (2015). A high- resolution simulation of groundwater and surface water over most of the continental US with the integrated hydrologic model ParFlow v3. *Geoscientific Model Development*, 8(3), 923– 937. https://doi.org/10.5194/gmd- 8- 923- 2015

Maxwell, R. M., Kollet, S. J., Smith, S. G., Woodward, C. S., Falgout, R. D., Ferguson, I. M., et al. (2014). ParFlow User's Manual. *International Ground Water Modeling Center Report GWMI*, 2010(1), 132.

Maxwell, R. M. & Miller, N. L. (2005). Development of a Coupled Land Surface and Groundwater Model. *Journal of Hydrometeorology*, 6, 233-247, https://doi.org/10.1175/JHM422.1

McGuire, K. J., & McDonnell, J. J. (2010). Hydrological connectivity of hillslopes and streams, Characteristic time scales and nonlinearities. *Water Resources Research*, 46(10). https://doi.org/10.1029/2010WR009341

Moretti, G., & Orlandini, S. (2018). Hydrography-Driven Coarsening of Grid Digital Elevation Models. *Water Resources Research*, 54(5), 3654-3672. https://doi.org/10.1029/2017WR021206

Orlandini, S., & Moretti, G. (2009a). Determination of surface flow paths from gridded elevation data. *Water Resources Research*, 45(3). https://doi.org/10.1029/2008WR007099

Orlandini, S., & Moretti, G. (2009b). Determination of surface flow paths from gridded elevation data. *Water Resources Research*, 45(3). https://doi.org/10.1029/2008WR007099

Orlandini, S., Moretti, G., Corticelli, M. A., Santangelo, P. E., Capra, A., Rivola, R., et al. (2012). Evaluation of flow direction methods against field observations of overland flow dispersion. *Water Resources Research*, 48(10). https://doi.org/10.1029/2012WR012067

Orlandini, S., Moretti, G., Franchini, M., Aldighieri, B., & Testa, B. (2003). Path-based methods for the determination of nondispersive drainage directions in grid-based digital elevation models. *Water Resources Research*, 39(6). https://doi.org/10.1029/2002WR001639

O'Neill, M. M. F., Tijerina, D. T., Condon, L. E., & Maxwell, R. M. (2021). Assessment of the ParFlow-CLM CONUS 1.0 integrated hydrologic model: evaluation of hyper-resolution water balance components across the contiguous United States. *Geoscientific Model Development,* 14(12), 7223-7254. https://doi.org/10.5194/gmd-14-7223-2021

Rahman, M., Sulis, M., & Kollet, S. J. (2016). Evaluating the dual-boundary forcing concept in subsurface-land surface interactions of the hydrological cycle. *Hydrological Processes*, 30(10), 1563-1573. https://doi.org/10.1002/hyp.10702

Richards, L. A., 1931: Capillary conduction of liquids through porous mediums. Physics, 1 , 318–333.

Soltani, S. S., Fahs, M., Bitar, A. A., & Ataie-Ashtiani, B. (2022). Improvement of soil moisture and groundwater level estimations using a scale-consistent river parameterization for the coupled ParFlow-CLM hydrological model: A case study of the Upper Rhine Basin. *Journal of hydrology*, 610, 127991. https://doi.org/10.1016/j.jhydrol.2022.127991

Sang, Y. F., Wang, Z., & Liu, C. (2014). Comparison of the MK test and EMD method for trend identification in hydrological time series. *Journal of Hydrology*. 510, 293-298. https://doi.org/10.1016/j.jhydrol.2013.12.039

Schalge, B., Haefliger, V., Kollet, S., & Simmer, C. (2019). Improvement of surface run-off in the hydrological model ParFlow by a scale-consistent river parameterization. *Hydrological Processes*, 33, 2006-2019. https://doi.org/10.1002/hyp.13448

Seck, A., Welty, C., & Maxwell, R. M. (2015). Spin-up behavior and effects of initial conditions for an integrated hydrologic model. *Water Resources Research*, 51(4), 2188-2210. https://doi.org/10.1002/2014WR016371

Tang, G. (2000). A Research on the Accuracy of Digital Elevation Models Science Press, Beijing.

Vázquez, R.F., Feyen, L., Feyen, J., & Refsgaard, J.C., 2002. Effect of grid size on effective parameters and model performance of the MIKE-SHE code. *Hydrological Processes*, 16(2), 355-372. https://doi.org/10.1002/hyp.334

Vanderlinden, K., Vereecken, H., Hardelauf, H., Herbst, M., Martínez, G., Cosh, M. H., et al. 2012. Temporal stability of soil water contents, A review of data and analyses. *Vadose Zone Journal*, 11(4). https://doi.org/10.2136/vzj2011.0178

Van Genuchten, M. T. (1980), A Closed-form Equation for Predicting the Hydraulic Conductivity of Unsaturated Soils. *Soil Science Society of America Journal*, 44, 892-898. https://doi.org/10.2136/sssaj1980.03615995004400050002x

Vereecken, H., Huisman, J. A., Pachepsky, Y., Montzka, C., vander,Kruk. J., Bogena, H., et al. 2014. On the spatio-temporal dynamics of soil moisture at the field scale. *Journal of Hydrology*, 516, 76-96. https://doi.org/10.1016/j.jhydrol.2013.11.061

Von, Gunten. D., Wöhling, T., Haslauer, C., Merchán, D., Causapé, J., Cirpka, O. A., et al. (2014). Efficient calibration of a distributed pde -based hydrological model using grid coarsening. *Journal of Hydrology*, 519, 3290-3304. https://doi.org/10.1016/j.jhydrol.2014.10.025

Yang, C., Li, H. Y., Fang, Y., Cui, C., Wang, T., Zheng, C., et al. (2020). Effects of Groundwater Pumping on Ground Surface Temperature, A Regional Modeling Study in the North China Plain. Journal of Geophysical Research. *Atmospheres*. 125(9). https://doi.org/10.1029/2019JD031764

Wu, Z., & Huang, N. E. (2004). A study of the characteristics of white noise

using the empirical mode decomposition method. Proceedings of the Royal Society of London. Series A: Mathematical, *Physical and Engineering Sciences*, 460(2046):1597-1611. https://doi.org/10.1098/rspa.2003.1221

Wu, Z., & Huang, N. E. (2005). Statistical significance test of intrinsic mode functions. In: Hilbert-Huang Transform and its Applications. *Interdisciplinary Mathematical Sciences*, 107-127. https://doi.org/10.1142/9789812703347_0005

Wu, Z., & Huang, N. E. (2009). Ensemble empirical mode decomposition: a noise-assisted data analysis method. *Advances in Adaptive Data Analysis*, 1 (01), 1-41. https://doi.org/10.1142/S1793536909000047

Zhang, Y. G., Schaap, M. G., & Zha, Y. Y. (2018). A high- resolution global map of soil hydraulic properties produced by a hierarchical parameterization of a physically based water retention model. *Water Resources Research*, 54, 9774-9790. https://doi.org/10.1029/2018WR023539

Zhou, G., Sun, Z., & Fu, S. (2016). An efficient variant of the Priority-Flood algorithm for filling depressions in raster digital elevation models. *Computers and Geosciences*. 90, 87-96. https://doi.org/10.1016/j.cageo.2016.02.021

Zhou, Q., & Chen, Y. (2011). Generalization of DEM for terrain analysis using a compound method. *ISPRS Journal of Photogrammetry and Remote Sensing*. 66(1), 38-45. https://doi.org/10.1016/j.isprsjprs.2010.08.005